

Thermoelectronic-wave coupling in laser photothermal theory of semiconductors at elevated temperatures

Andreas Mandelis,* MEMBER SPIE

Marios Nestoros

Constantinos Christofides

University of Cyprus

Faculty of Pure and Applied Sciences

Department of Natural Sciences

P.O. Box 537

CY-1678 Nicosia, Cyprus

E-mail: mandelis@me.utoronto.ca

Abstract. A quantitative analysis of linear temperature-dependent coupled thermoelectronic diffusion waves in the generation of the laser-induced IR photothermal radiometric signal from a photoexcited, plasma-wave-dominated, semi-infinite semiconductor Si wafer is presented. The strong coupling between the (usually assumed decoupled) carrier and thermal wave transport equations is accounted for explicitly and the range of violation of the Vasil'ev-Sandomirskii condition is studied. Thermoelectronic coupling is found to degrade the sensitivity of the plasma-originating IR radiometric signal in high-quality process Si substrates at elevated background temperatures and high modulation frequencies, with the exception of highly degenerate plasmas. © 1997 Society of Photo-Optical Instrumentation Engineers.

Subject terms: photoacoustic and photothermal science and engineering; semiconductors; laser photoexcitation; thermoelectronic wave; high temperatures.

Paper PPS-16 received May 10, 1996; revised manuscript received June 14, 1996; accepted for publication June 14, 1996.

1 Introduction

Laser-induced IR photothermal radiometry (PTR) has recently been established as a photothermal diagnostic technique with sensitivity to the dynamics of the photoexcited carrier plasma waves higher than other more conventional detection methods^{1,2} such as laser thermorefectance.³ In the rapidly growing literature of PTR detection of photoexcited carrier oscillations in semiconductors (called "plasma waves") driven by the absorbed optical fluence of an intensity-modulated laser emitting superbandgap photons, it has become clear⁴ that for certain classes of materials, such as high-quality, low-doping-level Si wafers, the plasma wave dominates the PTR signal, the magnitude of which is proportional to the recombination lifetime of the photoexcited carriers. The laser beam excitation generates a depth-dependent plasma wave $N(\mathbf{r},t)$, which propagates and recombines while emitting blackbody (Planck) radiation, usually captured by a wide-bandwidth IR detector. In addition, the plasma also contributes indirectly to the generation of a thermal wave diffusing in the semiconductor owing to thermal power release following nonradiative carrier recombination, and along with any direct lattice heating due to the absorption of the incident optical flux.⁵

The development of theoretical analyses of PTR signals (and other more general photothermal treatments of semiconductors⁶) is based on the treatment of plasma wave diffusion, which is usually assumed completely decoupled from any temperature oscillation effects. On the other hand, thermal wave diffusion includes a source term from the nonradiative decay of the photoexcited plasma. Recently,

Wagner and Mandelis⁷ have considered the coupling of plasma and thermal wave transport equations when nonlinear effects are present due to high-intensity pump laser irradiances. Nevertheless, the continuity equations when applied to plasma and heat conservation in a semiconductor readily show that at any laser fluence, the two transport equations are fully coupled⁸:

$$\frac{\partial \Delta N}{\partial t} = D_E \nabla^2 \Delta N - \frac{\Delta N}{\tau} + \frac{\partial n_0}{\partial T} \frac{\Delta T}{\tau} + \Phi \alpha F(t) \quad (1)$$

and

$$\frac{\partial \Delta T}{\partial t} = D_T \nabla^2 \Delta T + D_T \frac{E_g}{k} \frac{\Delta N}{\tau} + D_T \left(\frac{h\nu - E_g}{k} \right) \Phi \alpha F(t). \quad (2)$$

In the foregoing equations $\Delta N(\mathbf{r},t)$ is the excess photogenerated carrier plasma density; $\Delta T(\mathbf{r},t)$ is the excursion of the local temperature from the background value due to photothermal effects; D_E and D_T are the electronic (ambipolar) and thermal diffusivities, respectively; τ is the recombination lifetime of the semiconductor; n_0 is the equilibrium free-carrier density at temperature T ; Φ is the incident laser fluence; $F(t)$ is the temporal modulation function of the laser beam intensity; k is the thermal conductivity; E_g is the bandgap energy, and α is the optical absorption coefficient of the semiconductor at the laser excitation wavelength.

Vasil'ev and Sandomirskii⁹ first stated that, in the case of harmonic modulation function $F(t) = 1/2(1 + e^{i\omega t})$, the coupling term $(\partial n_0 / \partial T) \Delta T / \tau$ in Eq. (1) is negligible in the

*On leave from: University of Toronto, Photothermal and Optoelectronic Diagnostics Laboratories (PODL), Toronto, Ontario M5S 3G8, Canada.

case of relatively low temperatures, and generally when the equilibrium free-carrier density n_0 satisfies the inequality

$$n_0 \ll \frac{k}{k_B D_E} \left(\frac{k_B T}{E_g} \right)^2 \omega \tau [1 + (\omega \tau)^2]^{1/2}, \quad (3)$$

where k_B is Boltzmann's constant and ω is the angular modulation frequency. The quantity on the right-hand side of this inequality has the value $\approx 10^{16} \text{ cm}^{-3}$ for $\omega \tau = 10^{-4}$, and $\approx 10^{20} \text{ cm}^{-3}$ for $\omega \tau = 1$.

In this paper, analytical and computational consideration is given to the fully coupled pair of equations [Eqs. (1) and (2)], especially for the practical case of photothermal monitoring of the processing of semiconductors *in situ* under high-temperature ambient conditions and/or very low values of the product $\omega \tau$, where the coupling term may be significant. Therefore, this work is, in a sense, the generalization and extension of the earlier study by Nestoros et al.⁸ to much higher ambient temperature conditions than their $\leq 300 \text{ K}$. This is a rather low value for several important process steps, such as thermal annealing following ion implantation or thermal drive-in following diffusion.

2 Theory

2.1 IR Photothermal Radiometric Signal

IR PTR when applied to electronic materials yields signals originating in the blackbody emission from the semiconductor surface. Assuming an IR optical absorption coefficient increase due to the presence of photoinjected free carriers (FCs) [$\alpha'_{\text{IR}}(\mathbf{r}, \lambda) = \alpha_{\text{IR}}(\mathbf{r}, \lambda) + \Delta \alpha_{\text{FC}}(\mathbf{r}, \lambda)$], it can be shown that, in the case where the IR emission from FCs dominates the radiometric signal, the response of the IR detector is given by¹

$$\Delta Q(\lambda_{\text{VIS}}, T) = K(\lambda_1, \lambda_2, T) \int_0^L \Delta N(x, \lambda_{\text{VIS}}, T) dx, \quad (4)$$

where K is a temperature-dependent constant, L is the thickness of the semiconductor, and λ_{VIS} is the laser beam wavelength. Here λ_1 and λ_2 are the lower and upper cutoff IR wavelengths of the detector. A 1-D detection geometry is assumed, which holds when the size of the laser beam is large compared to the characteristic carrier diffusion length in the material. The constant K is given by^{1,10}

$$K(\lambda_1, \lambda_2, T) \equiv [1 - R(\lambda_{\text{VIS}})] \int_{\lambda_1}^{\lambda_2} [1 - R(\lambda)] \times \left(\frac{\lambda^2 q^3}{4 \pi^2 c^3 n \epsilon_0 m^2 \mu} \right) W_P(\lambda, T) d\lambda, \quad (5)$$

where R is the reflectivity of the surface at the excitation wavelength λ_{VIS} , or within the infrared bandwidth $[\lambda_1, \lambda_2]$ of the detector; q is the elementary charge; c is the speed of light; ϵ_0 is the dielectric constant of vacuum; n is the refractive index; and μ the mobility of free carriers in the semiconductor. Finally, $W_P(\lambda, T)$ is the Planck distribution function at ambient temperature T .

2.2 Coupled Thermoelectronic-Wave Equations

The FC density function $\Delta N(\mathbf{r}, t)$ in Eq. (4) can be calculated from Eqs. (1) and (2), on specifying the laser fluence modulation function $F(\omega t)$ for harmonic excitation of the plasma. The ac terms of the resulting equations are

$$D_E \nabla^2 \Delta N(r) - \left(i\omega + \frac{1}{\tau} \right) \Delta N(r) + \frac{1}{\tau} \frac{\partial n_0}{\partial T} \Delta T(r) = - \frac{\alpha P}{\pi W^2} e^{-\alpha z} \exp(-r^2/W^2) \quad (6)$$

and

$$D_T \nabla^2 \Delta T(r) - i\omega \Delta T(r) + \left(\frac{E_g}{\rho C} \right) \frac{\Delta N(r)}{\tau} = - \frac{\alpha P}{\pi W^2} \left(\frac{h\nu - E_g}{\rho C} \right) e^{-\alpha z} \times \exp(-r^2/W^2), \quad (7)$$

where P is the incident optical power, ρC is the product of the density and the specific heat of the solid, and W is the laser beam spotsize. The foregoing equations are generally strongly coupled. The spatial coordinate \mathbf{r} is assumed to be radially symmetric r at any depth z . The Hankel transforms of the carrier density and temperature oscillations can be written

$$n(\rho, z) = \int_0^\infty \Delta N(r, z) J_0(\rho r) \rho \, d\rho \quad (8)$$

and

$$\Theta(\rho, z) = \int_0^\infty \Delta T(r, z) J_0(\rho r) \rho \, d\rho. \quad (9)$$

Transforming Eqs. (6) and (7) into the Hankel domain, differentiating twice with respect to z the ensuing ordinary differential equations, and further substituting second derivatives from the original Hankel-transformed equations yields the following system of decoupled ordinary differential equations for the transforms of the plasma and thermal wave:

$$\frac{d^4 n(\rho, z)}{dz^4} - A(\rho) \frac{d^2 n(\rho, z)}{dz^2} + B(\rho) n(\rho, z) = G(\rho) e^{-\alpha z} \quad (10)$$

and

$$\frac{d^4 \Theta(\rho, z)}{dz^4} - A(\rho) \frac{d^2 \Theta(\rho, z)}{dz^2} + B(\rho) \Theta(\rho, z) = H(\rho) e^{-\alpha z}, \quad (11)$$

where the various coefficient dependencies on the Hankel parameter ρ are defined as follows:

$$A(\rho) \equiv 2\rho^2 + i\omega \left(\frac{1}{D_E} + \frac{1}{D_T} \right) + \frac{1}{D_E \tau} \quad (12)$$

and

$$B(\rho) \equiv \left(\rho^2 + \frac{i\omega}{D_T} \right) \left(\rho^2 + \frac{i\omega}{D_E} + \frac{1}{D_E\tau} \right) - \xi. \quad (13)$$

Here ξ represents the coupling term between thermal and electronic diffusive wave modes, a thermoelectronic wave quantity

$$\xi(T) \equiv \frac{1}{D_E\tau^2} \left(\frac{E_g}{k} \right) \frac{\partial n_0}{\partial T}. \quad (14)$$

Furthermore, the driving terms in Eqs. (10) and (11) are

$$G(\rho) = \frac{g(\rho)}{D_E} \left[\rho^2 + \frac{i\omega}{D_T} - \alpha^2 + \left(\frac{h\nu - E_g}{k\tau} \right) \frac{\partial n_0}{\partial T} \right] \quad (15)$$

and

$$H(\rho) = \frac{g(\rho)}{k} \left[\frac{E_g}{D_E\tau} + (h\nu - E_g) \left(\rho^2 + \frac{i\omega}{D_E} + \frac{1}{D_E\tau} - \alpha^2 \right) \right]. \quad (16)$$

The source function $g(\rho)$ represents the Hankel transform of the (assumed) Gaussian lateral laser beam profile:

$$g(\rho) = \frac{\alpha P}{2\pi} \exp(-\rho^2 W^2/4). \quad (17)$$

Only the solution of the Hankel transform of the plasma wave equation [Eq. (10)] is of interest in the context of the present PTR signal analysis from semiconductors with dominant plasma wave behavior. Using standard mathematical techniques, the solution to the homogeneous and complementary components of Eq. (10) for a semi-infinite semiconductor slab ($L \rightarrow \infty$) is found to be

$$n(\rho, z) = C_1(\rho) \exp[-Q(\rho)z] + C_2(\rho) e^{-\alpha z}, \quad (18)$$

where C_1 is an integration constant of the homogeneous solution and C_2 is given by the complementary solution:

$$C_2(\rho) \equiv g(\rho) \frac{M^2(\rho) - \alpha^2 + \tau D_E [(h\nu/E_g) - 1] \xi}{D_E \{ [M^2(\rho) - \alpha^2][\Lambda^2(\rho) - \alpha^2] - \xi \}}. \quad (19)$$

The exponent $Q(\rho)$ in Eq. (18) is the solution to a fourth-degree algebraic characteristic equation with four roots, as expected from the fourth-order Eq. (10). The chosen root is the one that gives the appropriate well-known¹¹ analytical solution to the reduced equation for $n(\rho, z)$ with $\xi=0$:

$$Q(\rho) = \left[\frac{1}{2} (\Lambda^2(\rho) + M^2(\rho)) + \{ [\Lambda^2(\rho) - M^2(\rho)]^2 + 4\xi \}^{1/2} \right]^{1/2}, \quad (20)$$

with

$$\Lambda(\rho) \equiv \left(\rho^2 + \frac{i\omega}{D_E} + \frac{1}{D_E\tau} \right)^{1/2} \quad (21)$$

and

$$M(\rho) \equiv \left(\rho^2 + \frac{i\omega}{D_T} \right)^{1/2}. \quad (22)$$

Finally, the unknown integration constant $C_1(\rho)$ can be uniquely determined from the Hankel transform of the usual boundary condition of carrier conservation at the surface $z=0$:

$$D_E \frac{dn(\rho, 0)}{dz} = sn(\rho, 0), \quad (23)$$

where s is the surface recombination velocity of the material. Equations (18) and (23) yield

$$C_1(\rho) = - \left[\frac{s + \alpha D_E}{s + Q(\rho) D_E} \right] C_2(\rho). \quad (24)$$

In the limit where $\xi=0$, Eq. (18) becomes

$$n(\rho, z; \xi=0) = \frac{g(\rho)}{D_E(\Lambda^2 - \alpha^2)} \left[e^{-\alpha z} - \left(\frac{s + \alpha D_E}{s + \Lambda D_E} \right) e^{-\Lambda z} \right], \quad (25)$$

which is the well-known solution of the Hankel transform of the decoupled transport equation for the plasma wave in the semi-infinite domain $z \geq 0$ (Ref. 12):

$$\frac{d^2 n(\rho, z)}{dz^2} - \Lambda^2(\rho) n(\rho, z) = - \frac{g(\rho)}{D_E} e^{-\alpha z}. \quad (26)$$

While Eq. (18) is valid for any diagnostic methodology that can monitor the plasma wave in a semiconductor, in the particular case of the PTR signal, the integral over the thickness of the wafer is required. Equation (4) then yields for the Hankel transform of the PTR signal ΔQ

$$q(\rho, \lambda_{\text{VIS}}) = K(\lambda_1, \lambda_2, T) C_2(\rho) \times \left\{ \frac{1}{\alpha} - \frac{1}{Q(\rho)} \left[\frac{s + \alpha D_E}{s + Q(\rho) D_E} \right] \right\}. \quad (27)$$

This equation can be used for numerical simulations of the photothermal radiometric response of semiconductors. As an example, a Si wafer will be considered for obtaining modulation frequency and temperature scan simulations. In the latter case, further consideration must be given to the T dependence of the integral definition of the coefficient $K(\lambda_1, \lambda_2, T)$ in Eq. (5). Use of the Planck radiation law for IR emission from surface area A of a blackbody emitter¹³ in Eqs. (4) and (5):

$$W_p(\lambda, T) = \frac{2\pi h}{\lambda^5} \frac{Ac^2}{\exp(hc/\lambda k_B T) - 1}, \quad (28)$$

assuming a weak T dependence of the IR reflectivity and an obvious change in the integration parameter λ , results in the following expression for K :

$$K(T) \approx \frac{[1 - R(\lambda_{\text{VIS}})](1 - \langle R \rangle) q^3 A k^2 \left[\frac{T^2}{\mu(T)} \right]}{2 \pi h c^3 n \epsilon_0 m^2} \times \int_{hc/\lambda_2 k_B T}^{hc/\lambda_1 k_B T} \frac{x dx}{e^x - 1}. \quad (29)$$

Here, $\langle R \rangle$ stands for the average value of the IR reflectivity over the detection bandwidth of the detector. The T dependence of the carrier mobility $\mu(T)$ depends on the physical mechanism controlling this parameter. Note that the spectral response of a broadband detector can be approximated by setting the limits of integration $[0, \infty)$ in Eq. (29). This would give a simple and relatively slow temperature dependence of the coefficient $K \propto T^2/\mu(T)$.

3 Application to Si Wafers under Processing Conditions

An important application of the foregoing thermoelectronic-wave theory occurs in the high-temperature processing of Si wafers. For highly doped substrates the inequality of Eq. (3) is unlikely to be valid, in which case the full theoretical results of Eqs. (27) and (29) must be implemented. Analytical inversion of the Hankel transform is impossible under these conditions. The Fortran 77 computer subroutine package "Gaussub" was used for all integrations involving the Hankel transformation. In proceeding with the simulations of the wafer temperature dependence of the PTR signal, it was assumed that the modulated temperature increase due to the absorption of the laser power is negligible compared to the ambient temperature. This is true in the case of good thermal conductors, such as Si. Therefore, the inversion of the solution transform Eq. (27) was performed in a stationary manner, i.e., with the background wafer temperature as a constant in each signal inversion case. Furthermore, the mild temperature dependence of $K(\lambda_1, \lambda_2, T)$ was omitted from the simulations to focus attention to material physical behavior only, away from the instrumental aspects of the photothermal detector.

3.1 Carrier Statistics in Si

The thermoelectronic coupling parameter ξ [Eq. (14)] depends on the temperature derivative of the background equilibrium free-carrier density $n_0(T)$, which is present in a semiconductor in the absence of external photoinjection of free nonequilibrium carriers. For the calculation of the free-electron density in the conduction band of intrinsic or n -type semiconductor Si, the following equation is used:¹⁴

$$n(T) = N_c F_{1/2}(\eta), \quad \eta(T) \equiv \frac{E_F(T) - E_g}{k_B T}, \quad (30)$$

where $N_c(T)$ is the effective density of states in the conduction band, $n(T)$ is the free-electron density, $E_F(T)$ is the Fermi energy, and $F_{1/2}$ is the Fermi integral of order 1/2, defined as

$$F_{1/2}(\eta) = \frac{2}{\sqrt{\pi}} \int_0^\infty \frac{E^{1/2} dE}{1 + \exp(E - \eta)}. \quad (31)$$

For intrinsic, extrinsic, and degenerate extrinsic Si (at high doping densities and high T), Blakemore¹⁵ presented the approximation for $F_{1/2}(\eta)$:

$$F_{1/2}(\eta) \approx \frac{e^{\eta(T)}}{1 + 0.27 e^{\eta(T)}}, \quad (32)$$

which is valid for $\eta < 1.3$ with an error $\leq \pm 3\%$. In the temperature range $300 \text{ K} \leq T \leq 1200 \text{ K}$, both intrinsic and extrinsic thermal excitations contribute to the FC density in Si. For the intrinsic excitation, the equality of free-electron and free-hole densities requires the right-hand side of Eq. (30) to be equal to $N_v \exp[-E_F(T)/k_B T]$, where N_v is the effective density of states in the valence band. Now Eqs. (30) and (32) result in a quadratic equation for $e^{\eta(T)}$, which in turn gives the following expression for the intrinsic density of free electrons:

$$n_{0i} = \{0.135a(T) + [0.0182a^2(T) + a(T)]^{1/2}\} \times \exp(-E_g/k_B T), \quad (33)$$

where $a(T)$ is given as a function of the ratio of the effective masses of free electrons and holes:

$$a(T) = (m_h^*/m_e^*)^{3/2} \exp(-E_g/k_B T). \quad (34)$$

For the extrinsic excitation, the right-hand side of Eq. (30) must be set equal to

$$n_{0e}(T) = \frac{N_d}{1 + \beta^{-1} \exp(\epsilon_d + \eta)}, \quad (35)$$

where N_d is the density of (the n -type) dopant; β is the degree of degeneracy of the bound state of the donor [taken to be 1/2 for Si (Ref. 14)]; and $\epsilon_d = E_d/k_B T$, with E_d being the donor state in the bandgap of the semiconductor. Combining Eqs. (30) and (35) yields a quadratic form for $e^{\eta(T)}$. Solving this equation results in the expression

$$n_{0e} = [2N_d N_c(T)] / (N_c(T) + 0.27N_d + \{[N_c(T) - 0.27N_d]^2 + 2N_d N_c(T) \exp(E_d/k_B T)\}^{1/2}) \quad (36)$$

for the density of extrinsic n -type carriers. Table 1 shows the ranges of η values for $n_{0i}(T)$ and $n_{0e}(T)$ for T between the two extremes considered in this paper, i.e., 300 and 1400 K and a wide range of dopant concentrations from the intrinsic limit to deep degeneracy. It can be seen that in all cases the error committed in calculating the FC densities remains within the 3% limit established by Blakemore.¹⁵ Based on the foregoing considerations, Fig. 1 shows the Arrhenius plot of the combined total FC density: $n_0(T) = n_{0i}(T) + n_{0e}(T)$, in Si ($E_g \approx 1.12 \text{ eV}$) using P doping, which creates a defect state in the bandgap at 45 meV from the bottom of the conduction band.¹⁶ The domination of the intrinsic thermal excitation at high temperatures is apparent for all but the highest doping density, $N_d = 1 \times 10^{20} \text{ cm}^{-3}$. In that degenerate case, it is also seen that the penetration of the Fermi level in the conduction band results in a measurable change in the slope of the extrinsic line.¹⁵ Equation (14) was evaluated by numerically differentiating the curves of Fig. 1 and the relevant values of $\xi(T)$ are

Table 1 Values of the Blakemore parameter $\eta(T)$ [Eq. (30)].

| N_d (cm^{-3}) | η (300 K) | η (1200 K) | η (1400 K) |
|----------------------------|----------------|-----------------|-----------------|
| 0 (intrinsic) | -22.034 | -3.981 | -3.021 |
| 10^{14} | -12.551 | -14.63 | -14.862 |
| 10^{16} | -7.946 | -10.025 | -10.257 |
| 10^{18} | -3.343 | -5.425 | -5.655 |
| 10^{20} | +1.138 | -1.089 | -1.295 |

shown in Fig. 2. It can be concluded from Fig. 2 that (1) the thermo-electronic wave parameter $\xi(T)$ spans an extremely wide range of values (up to 15 orders of magnitude for intrinsic and low-doping density substrates) between 300 and 1400 K in Si and (2) the strength of the coupling between thermal and electronic waves increases drastically with increasing doping density, especially at low temperatures.

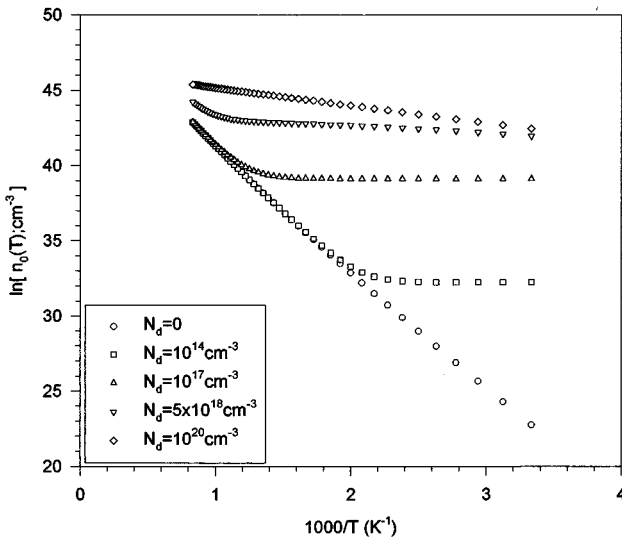
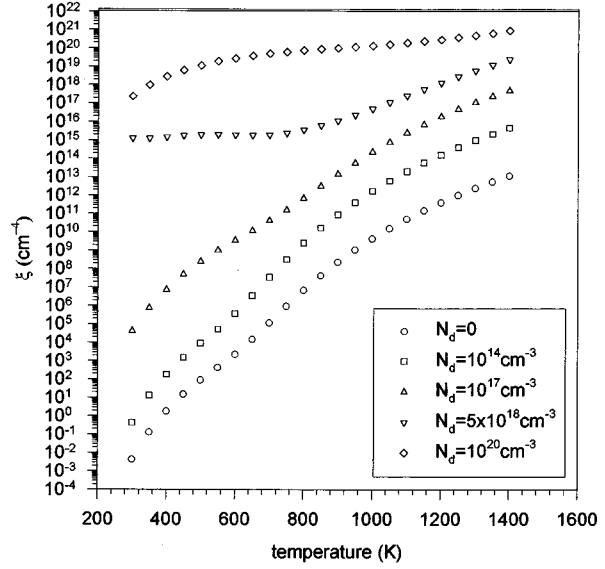
The temperature dependence of the remaining parameters in $\xi(T)$ for Si is as follows: the electron and hole mobilities (μ_e and μ_h) are related by the Einstein relation¹⁷

$$D_E = \left(\frac{k_B T}{q} \right) \frac{2\mu_e(T)\mu_h(T)}{\mu_e(T) + \mu_h(T)}. \quad (37)$$

The Si carrier mobilities as functions of doping density and temperature can be constructed on the basis of the empirical-fit relationship:¹⁸⁻²⁰

$$\mu(T) = \mu_{\min} + \frac{\mu_0}{1 + (N_d/N_{\text{ref}})^\alpha}, \quad (38)$$

where μ is the carrier mobility, N_d is the doping density (either acceptor or donor), and all other quantities are empirical-fit parameters that exhibit a temperature dependence of the form


Fig. 1 Arrhenius plots of the total FC density $n_0(T)$ for several P doping densities: $E_g = 1.12$ eV; $E_g - E_d = 45$ meV.

Fig. 2 Temperature dependence of the thermo-electronic coupling parameter $\xi(T)$ for P-doped Si at several dopant concentrations.

$$A = A_0 (T/300)^M, \quad (39)$$

where A_0 is a temperature-independent constant (the 300-K value of a parameter), and M is an exponent that is specific to a given parameter. Here N_{ref} , μ_{\min} , μ_0 , and α have the values $1.30 \times 10^{17} \text{ cm}^{-3}$, $92 \text{ cm}^2/\text{V s}$, $1268 \text{ cm}^2/\text{V s}$, and 0.91 , respectively, for electrons, and $2.35 \times 10^{17} \text{ cm}^{-3}$, $54.3 \text{ cm}^2/\text{V s}$, $406.9 \text{ cm}^2/\text{V s}$, and 0.88 , respectively, for holes.¹⁸

For doped samples, a temperature and concentration dependence must be introduced for the lifetime. As such, the empirical relationship was used^{18,21,22}:

$$\tau(T) = \frac{\tau_0}{1 + [n_{0i}(T) + n_{0e}(T)]/N_0}, \quad (40)$$

where $N_0 = 7.10 \times 10^{15} \text{ cm}^{-3}$; $n_{0i}(T)$ and $n_{0e}(T)$ are given by Eqs. (33) and (36), respectively; and $\tau_0 = 395 \text{ } \mu\text{s}$ is an empirically fit constant with dimensions of time. Equation (40) is not a universally valid relationship, but is indicative of the general nature of the doping dependence of τ . In our theoretical calculations, $\tau_0 = \tau_0(N_d)$, in the sense that the foregoing empirical value (originally valid for Si solar cells) has been multiplied by a constant for each doping density so as to yield accepted literature values at room temperature (e.g., Ref. 14, Chap. 6).

In the case of intrinsic Si, the recombination time is mainly due to deep-level traps. The temperature dependence of the surface recombination velocity was related to the surface recombination lifetime²³:

$$s(T) = \left[\frac{D_E(T)}{\tau_s(T)} \right]^{1/2}. \quad (41)$$

In writing Eq. (41) it was assumed that the photon wavelength is such that photoexcitation of the semiconductor occurs at, or very near, the surface (e.g., Si with the 488- or 514-nm lines of the Ar-ion laser); in this case, the value of

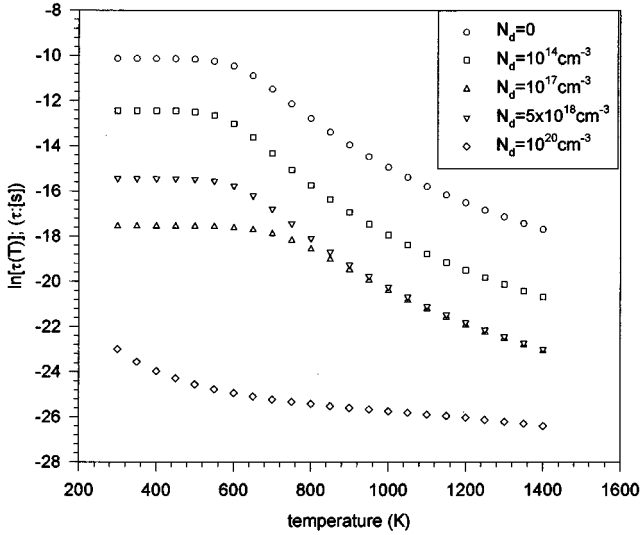


Fig. 3 Temperature dependence of the carrier lifetime in *P*-doped Si with doping density as a parameter: τ_0 values are $39.5 \mu\text{s}$ ($N_d=0$), $3.95 \mu\text{s}$ ($N_d=10^{14} \text{ cm}^{-3}$), $0.356 \mu\text{s}$ ($N_d=10^{17} \text{ cm}^{-3}$), and 39.5 ns ($N_d=10^{20} \text{ cm}^{-3}$).

the active lifetime is controlled by the electronic condition of the surface,²⁴ which justifies the tacit assumption $\tau = \tau_s$ behind Eq. (41). Figure 3 shows the temperature dependence of the electronic lifetimes in Si with doping density as a parameter and an adjusted value of the constant τ_0 , as already discussed, so as for Eq. (40) to yield realistic experimental results. In the intrinsic case where $N_d=0$, $\tau_0=39.5 \mu\text{s}$ at $T=300 \text{ K}$ (Ref. 24). The decrease of τ with increasing temperature and doping density is expected owing to the presence of higher FC concentrations and empty states, which thus facilitates the recombination mechanism. The increase in the surface recombination velocity with increasing temperature is not as significant as that of $\tau(T)$, due to the square root dependence of Eq. (41).

For the optical absorption coefficient in Si as a function of wavelength and temperature, the approximate expression was adopted^{17,25}:

$$\alpha \text{ (cm}^{-1}\text{)} = 6000 \left\{ \frac{[h\nu - E_g(T) - 0.0575]^2}{1 - \exp(-670/T)} + \frac{[h\nu - E_g(T) + 0.0575]^2}{\exp(670/T) - 1} \right\}. \quad (42)$$

The bandgap energy $E_g(T)$ is described by the following expression¹⁷:

$$E_g(T) \text{ (eV)} = 1.16 - \frac{7.02 \times 10^{-4} T^2}{T + 1108}. \quad (43)$$

Finally, the temperature dependence of the thermal conductivity $k(T)$ in Eq. (14) was obtained from²⁶

$$k(T) \text{ (W/cm K)} = 1.35 \left(\frac{T}{300} \right)^{-1.12}. \quad (44)$$

Table 2 Comparison between n_0 and Q [Eq. (3)] for intrinsic and extrinsic Si at $f=100 \text{ Hz}$ and 1 MHz , and at $T=300$ and 1400 K .

| f (Hz) | T (K) | N_d (cm^{-3}) | $Q(f, T)$ (cm^{-3}) | n_0 (cm^{-3}) |
|----------|---------|----------------------------|--------------------------------|----------------------------|
| 10^2 | 300 | 0 (intrinsic) | 7.394×10^{16} | 1.168×10^{10} |
| 10^2 | 1400 | 0 (intrinsic) | 1.53×10^{15} | $1.37 \times 10^{19*}$ |
| 10^6 | 300 | 0 (intrinsic) | 1.834×10^{23} | 1.168×10^{10} |
| 10^6 | 1400 | 0 (intrinsic) | 1.543×10^{19} | $1.37 \times 10^{19*}$ |
| 10^2 | 300 | 10^{14} | 7.394×10^{15} | 1.214×10^{10} |
| 10^2 | 1400 | 10^{14} | 7.638×10^{13} | $1.375 \times 10^{19*}$ |
| 10^6 | 300 | 10^{14} | 1.837×10^{21} | 1.214×10^{10} |
| 10^6 | 1400 | 10^{14} | 7.638×10^{17} | $1.375 \times 10^{19*}$ |
| 10^2 | 300 | 10^{17} | 6.243×10^{13} | $9.833 \times 10^{16*}$ |
| 10^2 | 1400 | 10^{17} | 7.169×10^{12} | $1.273 \times 10^{19*}$ |
| 10^6 | 300 | 10^{17} | 6.314×10^{17} | 9.833×10^{16} |
| 10^6 | 1400 | 10^{17} | 7.169×10^{16} | $1.273 \times 10^{19*}$ |
| 10^2 | 300 | 10^{20} | 1.893×10^{12} | $2.705 \times 10^{18*}$ |
| 10^2 | 1400 | 10^{20} | 3.901×10^{11} | $6.89 \times 10^{19*}$ |
| 10^6 | 300 | 10^{20} | 1.893×10^{16} | $2.705 \times 10^{18*}$ |
| 10^6 | 1400 | 10^{20} | 3.901×10^{15} | $6.89 \times 10^{19*}$ |

3.2 Frequency Behavior of a Coupled Thermoelectronic Wave

In the light of the inequality of Eq. (3), a numerical investigation of its validity at the extreme temperatures $T=300 \text{ K}$ and $T=1400 \text{ K}$ was undertaken and, subsequently, complete calculations were carried out to confirm its predictions. Symbolizing the right-hand side of the inequality by a quantity $Q(f, T)$ in units of an effective carrier density (cm^{-3}), Table 2 shows with an asterisk in which cases Vasil'ev and Sandomirskii⁹ have predicted that the thermoelectronic-wave coupling may *not* be negligible in a photoexcited semiconductor. These are all the high-temperature and the $N_d > 10^{17} \text{ cm}^{-3}$ situations. This table shows that even for intrinsic and very low dopant concentrations at elevated temperatures, and/or for moderate doping densities at room temperature, thermoelectronic-wave coupling may be important in semiconductors. The latter case is, of course, in direct contradiction to most theoretical treatments of the photothermal effects in semiconductors.^{6-12,23,24,27} Certainly, Table 2 demonstrates that all theoretical models must consider the coupled thermoelectronic wave diffusion when treating photothermal phenomena in semiconductors at elevated temperatures, such as required for device processing. For this reason, the temperature and frequency dependences of the photothermal radiometric signal were considered in some detail, especially in the parameter ranges of outright violation of the inequality of Eq. (3). In the following simulations, the thermal wave component of the signal following the thermalization of the FC wave represented by Eqs. (7) and (11) is ignored, as it is negligible with high-quality materials that have not undergone surface damage or implantation.^{10,27}

The radiometric frequency response of a Si wafer is given by the Hankel transform of Eq. (27) at a fixed background temperature. The resulting amplitude curves for a 1-mm spotsize laser beam at $T=300 \text{ K}$ were similar to those presented by Sheard et al.,²⁷ and the phase curves

also coincided with those calculated by Salmick et al.¹ Those authors used a 1-D model of the radiometric signal without thermo-electronic-wave coupling, i.e., $\xi=0$. Results similar to earlier 3-D ones by Sheard¹⁰ and Sheard et al.²⁷ were further obtained with a 1.5- μm spotsize beam, which clearly falls into the 3-D radiometric signal detection. No changes in the frequency response could be observed on account of the coupling coefficient ξ , thus verifying the adequacy of existing decoupled theoretical models⁶⁻¹² for room T studies of low-doped Si. At room temperature, the simulated Si samples with elevated doping density, $N_d > 10^{17} \text{ cm}^{-3}$, exhibited decreased PTR amplitude and a phase shift with respect to the conventional decoupled theory, represented by the Hankel transform of Eq. (25). Figure 4 shows the frequency response for $N_d = 5 \times 10^{18} \text{ cm}^{-3}$. For the same photon incidence rate on the semiconductor surface, a smaller density of bound carriers will be available in the impurity state and across the bandgap for optical excitation, owing to the upward shift of the Fermi level induced thermally by the coupling coefficient ξ . The result is a smaller radiometric amplitude, indicating a decreased photoexcitation quantum yield, compared to the $\xi=0$ case. The flatness of the amplitude is due to the decrease in the recombination time τ at increased doping densities, so that the turning point at $\omega\tau \approx 1$ has been shifted to higher frequencies outside the conventional experimental 1-MHz range. Similar effects can be seen when the laser beam spotsize increases to 1 mm, with the conclusion that the dimensionality of the problem is not a major factor in the coupled thermo-electronic wave behavior. The dimensionality is expected to be important, however, in the evolution of the thermal wave component of the IR radiometric signal, which has been ignored in this treatment. Note that the phase shift of Fig. 4(b) is toward negative values, i.e., it is a phase lag with respect to the decoupled case. On the other hand, the simulation for $N_d = 10^{20} \text{ cm}^{-3}$ exhibits a positive phase shift, i.e., a lead. The former phase lag is due to the plasma wave density centroid moving deeper into the bulk, as enhanced conversion to thermal wave power occurs due to the thermo-electronic coupling; the latter phase lead is due to the combination of the saturation of the plasma wave component with respect to the recombination lifetime τ at very high doping densities ($\omega\tau \ll 1$), and the much increased surface recombination velocity s , which depletes the active carriers, thus shifting the plasma density centroid farther toward the surface, albeit at much decreased carrier density and, consequently, signal strength (a decrease of five orders of magnitude in relative signal level from that of Fig. 4 was calculated). Figure 5 shows the surface recombination velocity profiles as functions of ambient temperature for various P -doping densities in Si.

In view of the results of Fig. 4 and the foregoing discussion, medium- to high-doping density processes must take into account the thermo-electronic-wave coupling during the photothermal analysis of data, even under room-temperature conditions.

For dopant concentration $N_d = 5 \times 10^{18} \text{ cm}^{-3}$ the phase shift behavior changes from lag to lead between $T = 800$ and 1400 K, whereas for higher concentrations the phase shift is always a lead, irrespective of the ambient temperature in the $300 \leq T \leq 1400$ K range, as expected from the rapidly rising surface recombination velocity of Fig. 5. The

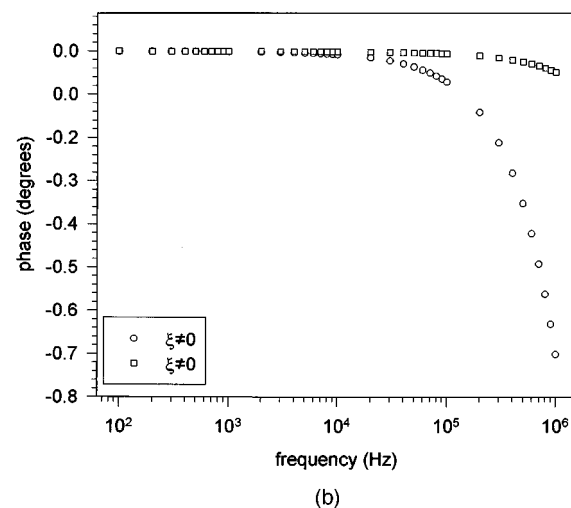
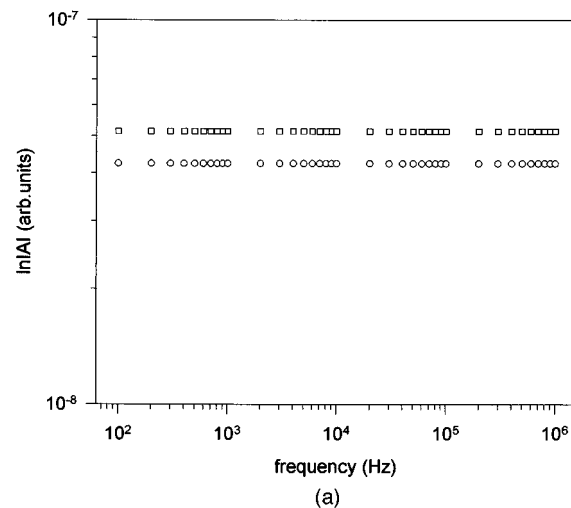


Fig. 4 Frequency response of a Si wafer calculated with conventional ($\xi=0$) and coupled ($\xi>0$) theory: $T=300$ K, $W=1.5 \mu\text{m}$, and $N_d=5 \times 10^{18} \text{ cm}^{-3}$.

thermo-electronic-wave coupling is, of course, stronger at high temperatures (Fig. 2); as a result, the decrease of the relative signal amplitude with respect to the uncoupled case is more pronounced than at low temperatures, while the absolute value of the amplitude decreases by several orders of magnitude due to enhanced recombination, as shown in Fig. 6 and in comparison with Fig. 4.

For intrinsic Si, the thermo-electronic-wave coupling induces a phase lag at $T=1200$ K, which, if not accounted for, could be mistaken as due to a longer recombination lifetime, thus yielding an erroneous value for that quantity, as shown in Fig. 7.

3.3 Temperature Behavior of Coupled Thermo-electronic Waves

Calculations involving several P -doping densities in Si as functions of ambient temperature T were carried out and are presented in Fig. 8. The carrier ambipolar diffusivity and the material optical absorption coefficient as functions of temperature are shown in Figs. 9 and 10, respectively. Two main T regimes may be identified in Fig. 8: a low T

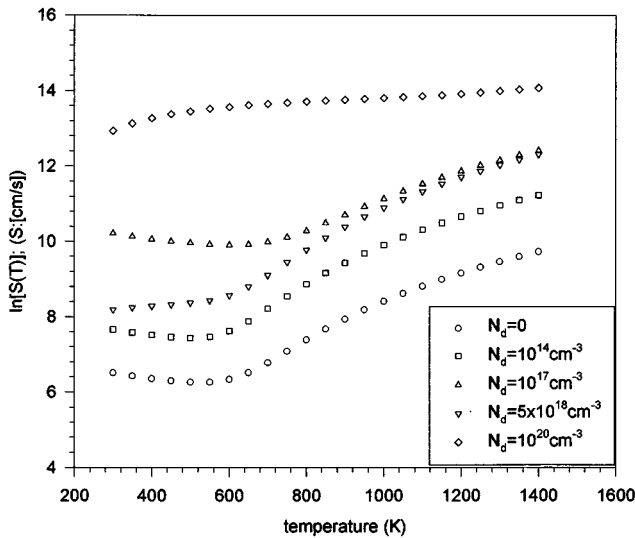


Fig. 5 Surface recombination velocity versus temperature for intrinsic and extrinsic *P*-doped Si, including the degenerate case of $N_d=10^{20} \text{ cm}^{-3}$.

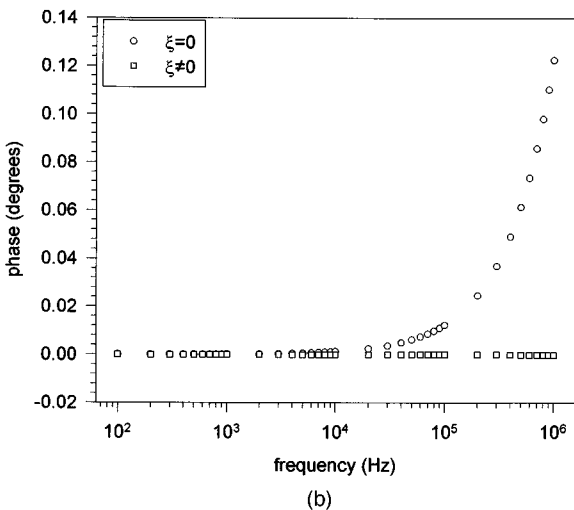
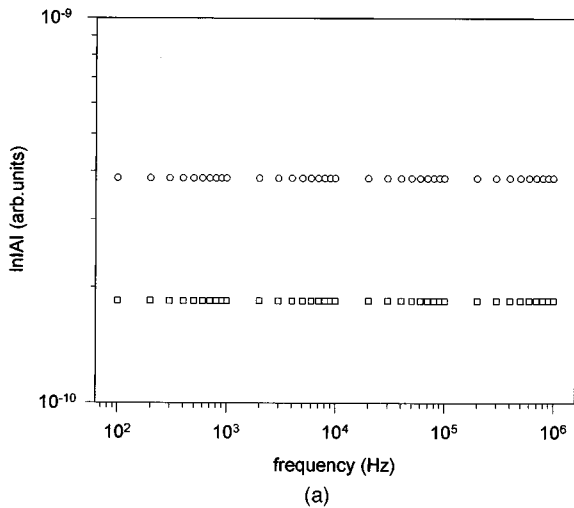


Fig. 6 Frequency response of a Si wafer calculated with conventional ($\xi=0$) and coupled ($\xi>0$) theory: $T=1200 \text{ K}$, $W=1.5 \mu\text{m}$, and $N_d=5 \times 10^{18} \text{ cm}^{-3}$.

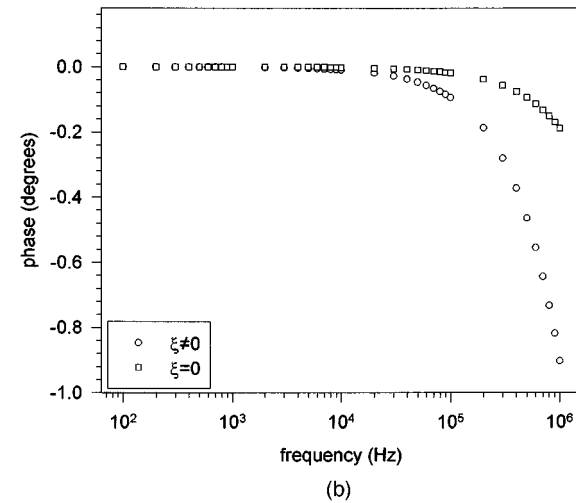
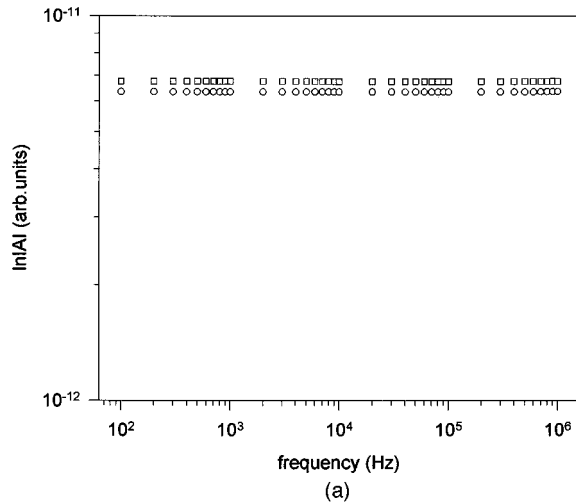


Fig. 7 Frequency response of an intrinsic Si wafer calculated with conventional ($\xi=0$) and coupled ($\xi>0$) theory: $T=1200 \text{ K}$ and $W=1 \text{ mm}$.

range below $\sim 700 \text{ K}$ and a high T range between 700 and 1400 K . For intrinsic Si, the rising temperature from the reference level $T=300 \text{ K}$ incurs an increase in the signal amplitude as more carriers become thermally ionized and enter the free (conduction) band. As the temperature increases further, the steep decrease in recombination lifetime (Fig. 3) decreases the net density of FCs, thus producing a broad maximum in the amplitude. This is accompanied by another extremum (minimum) in the signal phase [Fig. 8(b)] saturating at 0 deg at high T , as the carrier plasma centroid moves toward the material surface under conditions of accelerated recombination and as the absorption coefficient increases, thus localizing the photoexcited carrier source closer to the surface. A similar behavior is observed for lightly doped Si, $N_d=10^{14} \text{ cm}^{-3}$, with a more pronounced amplitude decrease and steeper phase saturation at 0 deg in the high T range, due to the significantly smaller τ than the intrinsic case. As a result, the extrema in both amplitude and phase are located at lower T than the intrinsic material. The situation with $N_d=10^{17} \text{ cm}^{-3}$, produces a lower overall signal than the foregoing curves, owing to the measurable increase in surface recombination

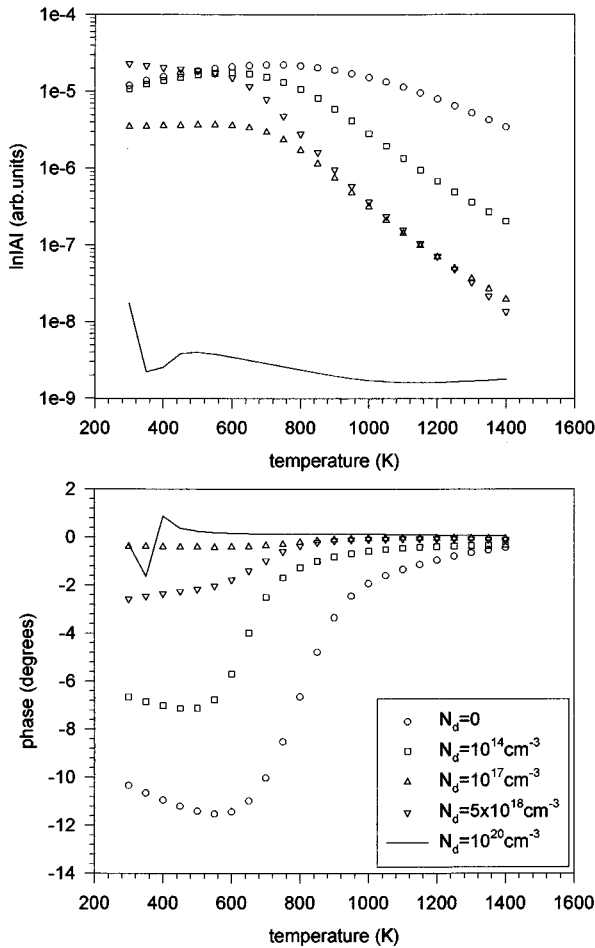


Fig. 8 Temperature dependences of plasma wave amplitude and phase of P-doped Si wafers with various doping densities and thermoelectronic-wave coupling: $W=1.5 \mu\text{m}$ and $f=10^5 \text{ Hz}$.

velocity (Fig. 5) and the further decrease in the values of τ due to enhanced recombination in the presence of higher densities of impurity states. It is interesting to note the inversion in signal amplitude for $N_d=5 \times 10^{18} \text{ cm}^{-3}$ at low T . This occurs because of the very steep drop in the value of the ambipolar diffusion coefficient D_E for this case (Fig. 9). This effect helps localize the FCs near the surface, thus increasing the effective density (and the signal strength) compared to the previous cases. At high temperatures the steep lifetime drop becomes responsible for the crossover between the $N_d=10^{17}$ and $5 \times 10^{18} \text{ cm}^{-3}$ cases. Finally, the very low lifetime associated with the degenerate doping case ($N_d=10^{20} \text{ cm}^{-3}$) generally depresses the magnitude of the signal substantially, but not monotonically: The strong thermoelectronic-wave coupling and the surface recombination cause a steep decay at low T , which, however, is reversed at intermediate temperatures owing to the increasing thermally generated FC density from degenerate states in the conduction band, increasing diffusivity and near-surface optical absorption efficiency (coefficient). At very high temperatures, the nearly metallic character of the semiconductor saturates the amplitude, despite the very efficient thermal recombination. The effect of the thermoelectronic-wave coupling coefficient $\xi(T)$ in this de-

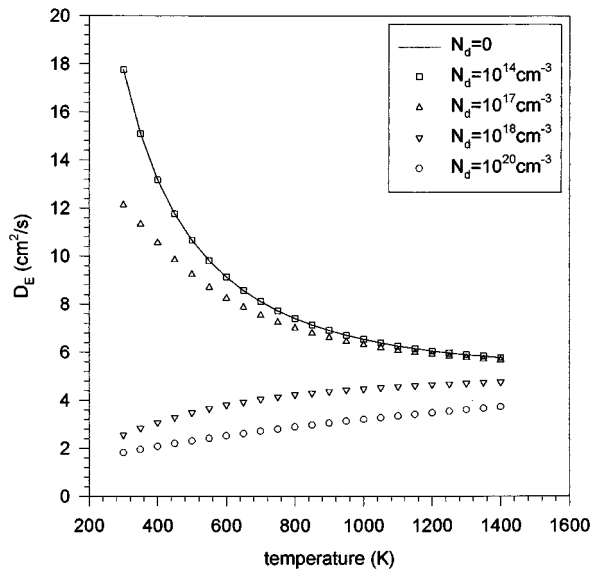


Fig. 9 Carrier diffusivity dependence on temperature [Eq. (37)].

generate case is shown in Fig. 11. Besides the overall decrease in signal amplitude due to enhanced thermal recombination in the case $\xi > 0$, the counteracting effects of thermal decay versus thermal generation clearly produce the amplitude and phase extrema in the range $T \leq 800 \text{ K}$. At very high temperatures the amplitude crossover is due to the degenerate condition of this material: the coupling coefficient ξ increases the density of deexcited carriers, which, however, are immediately available within the conduction band as FCs, thus resulting in the amplitude enhancement observed in Fig. 11. This implies that thermoelectronic-wave coupling may, indeed, increase photothermal signal levels at very high temperatures compared to the uncoupled case.

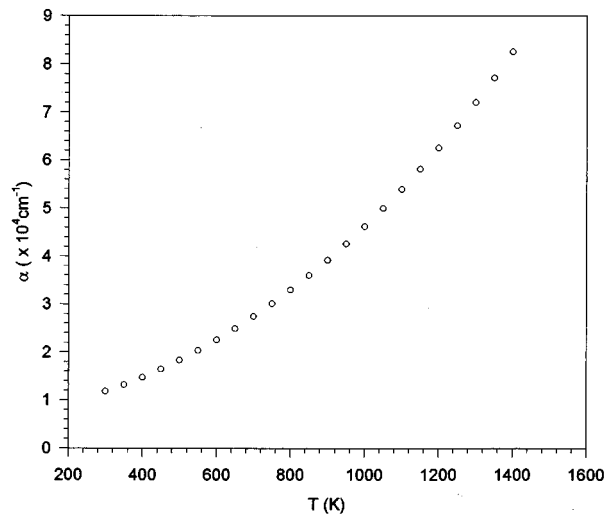


Fig. 10 Optical absorption coefficient dependence on temperature [Eq. (42)].

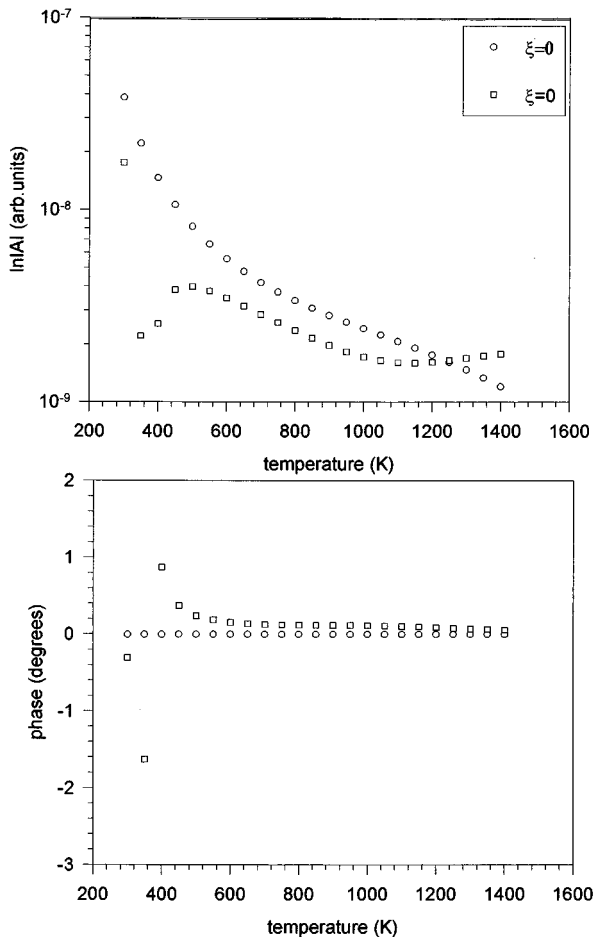


Fig. 11 Comparison between uncoupled ($\xi=0$) and coupled ($\xi>0$) theory of the temperature dependence of degenerate Si with $N_d=10^{20} \text{ cm}^{-3}$, $f=10^5 \text{ Hz}$, and $W=1.5 \mu\text{m}$.

4 Conclusions

A theoretical model for the behavior of the fully coupled plasma and thermal wave transport equations of photoexcited plasma waves in semiconductors was constructed. For the first time, this theory enabled the study of the effect of the resulting thermo-electronic-wave coupling term on plasma wave transport as a function of doping density and temperature in the range of violation of the Vasil'ev and Sandomirskii inequality [Eq. (3)], ignoring the thermal wave component in the IR photothermal radiometric signal detection mode. It was found that the coupling term negatively influences the strength of the signal, except with the fully degenerate plasma wave case at very high temperatures and must be taken into account for accurate measurements of lifetimes and electronic diffusivities.

References

1. A. Salmick, C. Jean, and A. Mandelis, "Non-contacting photothermal radiometry of SiO_2/Si MOS capacitor structures," *Solid State Electron.* (in press).
2. A. Othonos, C. Christofides, and A. Mandelis, "Photothermal radiometric investigation of implanted silicon: the influence of dose and thermal annealing," *Appl. Phys. Lett.* **69**, 821–823 (1996).
3. A. Rosenzweig, "Thermal wave characterization and inspection of semiconductor materials and devices," in *Photoacoustic and Thermal*

4. *Wave Phenomena in Semiconductors*, A. Mandelis, Ed., pp. 97–136, North-Holland, New York (1987).
5. S. Sheard and M. Somekh, "Photothermal radiometry of semiconductors," Chap. 5 in *Progress in Photothermal and Photoacoustic Science and Technology*, Vol. II: *Non-Destructive Evaluation*, A. Mandelis, Ed., pp. 111–150, PTR Prentice-Hall, Englewood Cliffs, NJ (1994).
6. A. Mandelis, A. Budiman, and M. Vargas, "Photothermal deep level transient spectroscopy of impurities and defects in semiconductors," in *Semiconductors and Semimetals: Effects of Disorder and Defects in Ion-Implanted Semiconductors; Optical and Photothermal Characterization*, C. Christofides and G. Ghibaudo, Eds. (in press).
7. A. Mandelis, Ed., *Photoacoustic and Thermal Wave Phenomena in Semiconductors*, North-Holland, New York (1987).
8. R. E. Wagner and A. Mandelis, "Nonlinear photothermal modulated optical reflectance and photocurrent phenomena in crystalline semiconductors: I. theoretical," *Semicond. Sci. Technol.* **11**, 289–299 (1996); R. E. Wagner and A. Mandelis, "Nonlinear photothermal modulated optical reflectance and photocurrent phenomena in crystalline semiconductors: II. experimental," *Semicond. Sci. Technol.* **11**, 300–307 (1996).
9. M. Nestoros, B. C. Forget, C. Christofides, and A. Seas, "Photothermal reflection versus temperature: quantitative analysis," *Phys. Rev. B* **51**, 14115–14123 (1995).
10. A. N. Vasil'ev and V. B. Sandomirskii, "Photoacoustic effects in finite semiconductors," *Sov. Phys. Semicond.* **18**, 1095–1099 (1984).
11. S. J. Sheard, "Photothermal radiometric microscopy," PhD Thesis, University College, London (1987).
12. B. C. Forget, "Caractérisation des Propriétés de Transport Electronique du Silicium par des Méthodes Photothermiques," Chap. 3, PhD Thesis, Univ. Pierre et Marie Curie, Paris (1993).
13. D. Fournier and A. C. Boccara, "Photothermal investigations of solids: basic physical principles," *Photoacoustic Investigations of Solids and Fluids*, J. A. Sell, Ed., pp. 35–79, Academic, New York (1989).
14. F. Grum and R. J. Becherer, *Optical Radiation Measurements*, Vol. 1, p. 105, Academic, New York (1979).
15. J. S. Blakemore, *Semiconductor Statistics*, Chap. 2, Dover, New York (1987).
16. J. S. Blakemore, "Some applications and properties of the Fermi-Dirac integrals," in *Semiconductor Statistics*, Appendix C, pp. 354–365, Dover, New York (1987).
17. C. Kittel, *Introduction to Solid State Physics*, Chap. 8, 5th ed., Wiley, New York (1984).
18. S. M. Sze, *Physics of Semiconductor Devices*, Wiley, New York (1965).
19. R. F. Pierret, "Recombination-generation processes," Chap. 5 in *Advanced Semiconductor Fundamentals*, Vol. VI, R. F. Pierret and G. W. Neudeck, Eds., pp. 183–193, Addison-Wesley, Reading, MA (1987).
20. D. M. Caughey and R. F. Thomas, "Carrier mobility in silicon empirically related to doping and field," *Proc. IEEE* **55**, 2192–2197 (1967).
21. D. N. Arora, J. R. Hauser, and D. J. Roulston, "Electron and hole mobilities in silicon as a function of concentration and temperature," *IEEE Trans. Electron Devices* **ED-29**, 292–296 (1982).
22. J. G. Fossum, "Computer-aided numerical analysis of silicon solar cells," *Solid State Electron.* **19**, 269–274 (1976).
23. J. G. Fossum, "Physical operation of back-surface-field silicon solar cells," *IEEE Trans. Electron Devices* **ED-24**, 322–327 (1977).
24. Z. H. Chen, R. Bleiss, A. Mandelis, and F. Shimura, "Photothermal rate-window spectrometry for non-contact bulk lifetime measurements in semiconductors," *J. Appl. Phys.* **73**, 5043–5048 (1993).
25. A. Mandelis, R. Bleiss, and F. Shimura, "Highly-resolved separation of carrier and thermal-wave contributions to photothermal signals from Cr-doped silicon using rate-window infrared radiometry," *J. Appl. Phys.* **74**, 3431–3434 (1993).
26. A. Lietoila, R. B. Gold, and J. F. Gibbons, "Temperature rise in Si by continuous xenon arc lamp radiation," *J. Appl. Phys.* **53**, 1169–1172 (1982).
27. J. R. Meyer, M. R. Kruer, and F. J. Bartoli, "Optical heating in semiconductors: laser damage in Ge, Si, InSb, and GaAs," *J. Appl. Phys.* **51**, 5513–5522 (1980).
28. S. J. Sheard, M. G. Somekh, and T. Hiller, "Non-contacting determination of carrier lifetime and surface recombination velocity using photothermal radiometry," *Mater. Sci. Eng. B* **5**, 101–105 (1990).

Biographies and photographs of the authors appear in the paper "Laser photothermal diagnostics of genuine and counterfeit British and United States banknotes" in this issue.